25-Day Period Large-Scale Oscillations in the Argentine Basin Revealed by the TOPEX/Poseidon Altimeter

LEE-LUENG FU AND BENNY CHENG

Jet Propulsion Laboratory, California Institute of Technology, Pasadena, California

BO QIU

Department of Oceanography, University of Hawaii, Honolulu, Hawaii

(Manuscript received 19 July 1999, in final form 27 April 2000)

ABSTRACT

The measurement of the global sea surface height made by the TOPEX/Poseidon satellite has provided the first synoptic view of large-scale oceanic variability at intraseasonal scales from weeks to months. Areas of significant intraseasonal variability were found primarily in the Tropics and the high-latitude oceans, the Southern Ocean in particular. The focus of the paper is the finding of large-scale oscillations at a period of 25 days in the Argentine Basin of the South Atlantic Ocean. These oscillations exhibit a dipole pattern of counterclockwise rotational propagation centered at 45°S, 317°E over the Zapiola Rise. The scale of the dipole is about 1000 km. The peak-to-trough amplitude is on the order of 10 cm. The amplitude of these oscillations has large seasonal-to-interannual variations. These oscillations are shown to be associated with a free barotropic mode of the basin as a solution to a linearized barotropic vorticity equation. Closed f/H contours provide a mechanism for the confinement of the waves to the topographic feature of the Zapiola Rise. Results from a numerical model simulation reproduced the patterns of the observed oscillations. The resultant mass transport variability is on the order of 50 Sv (Sv $\equiv 10^6$ m^3 s^{-1}). Deep current meters in the Argentine Basin reveal signals consistent with the altimetry observations.

1. Introduction

Intraseasonal variability of sea level, characterized by timescales ranging from a few days to a season and by spatial scales larger than 500 km (roughly the upper bound of the mesoscale), has not been well observed until the advent of precision altimetric missions such as TOPEX/Poseidon (T/P: Fu et al. 1994). In situ observations in the Tropics are an exception for several reasons, however. First, most island tide gauges are located in the Tropics, providing a database for describing the variability. Second, the intraseasonal variability of the tropical oceans is fairly energetic. Third, the mesoscale eddies, which are an impediment to observing the intraseasonal scales, are relatively weak in the Tropics. The tropical intraseasonal variability has been interpreted primarily as the ocean's response to atmospheric forcing in terms of internal gravity waves as well as Kelvin, Rossby, and instability waves (e.g., Wunsch and Gill 1976; Enfield 1987; McPhaden 1996). The sparsely populated in situ observations at mid and high latitudes are not adequate for a detailed description of the intraseasonal variability because the large-scale signals are often contaminated by the ubiquitous mesoscale eddies, which are difficult to remove from the in situ observations. Using a large number of deep current meter observations, Koblinsky et al. (1989) demonstrated the existence of large-scale response of the ocean to local wind forcing at intraseasonal scales. Other studies reported evidence of remotely forced large-scale response of the ocean to wind forcing as barotropic Rossby waves (Brink 1989; Niiler et al. 1993; Samelson 1990; Luther et al. 1990). However, the in situ observations analyzed in these studies were not able to provide a coherent, synoptic view of the large-scale variabilities.

With its unique spatial and temporal sampling capability, satellite altimetry offers an effective approach to the problem. However, the relatively low amplitude (typically less than 10 cm) and large scales (greater than 500 km) of the variability present a challenge to the performance of altimetric measurement. Before the advent of the T/P mission, the orbit errors in altimetric measurement are much larger than 10 cm. Because the spatial scales of the orbit errors were rather large (predominantly on the order of the circumference of Earth), small-scale signals could be preserved after the removal

Corresponding author address: Dr. Lee-Lueng Fu, MS 300-323, Jet Propulsion Laboratory, California Institute of Technology, 4800 Oak Grove Dr., Pasadena, CA 91109-8099.

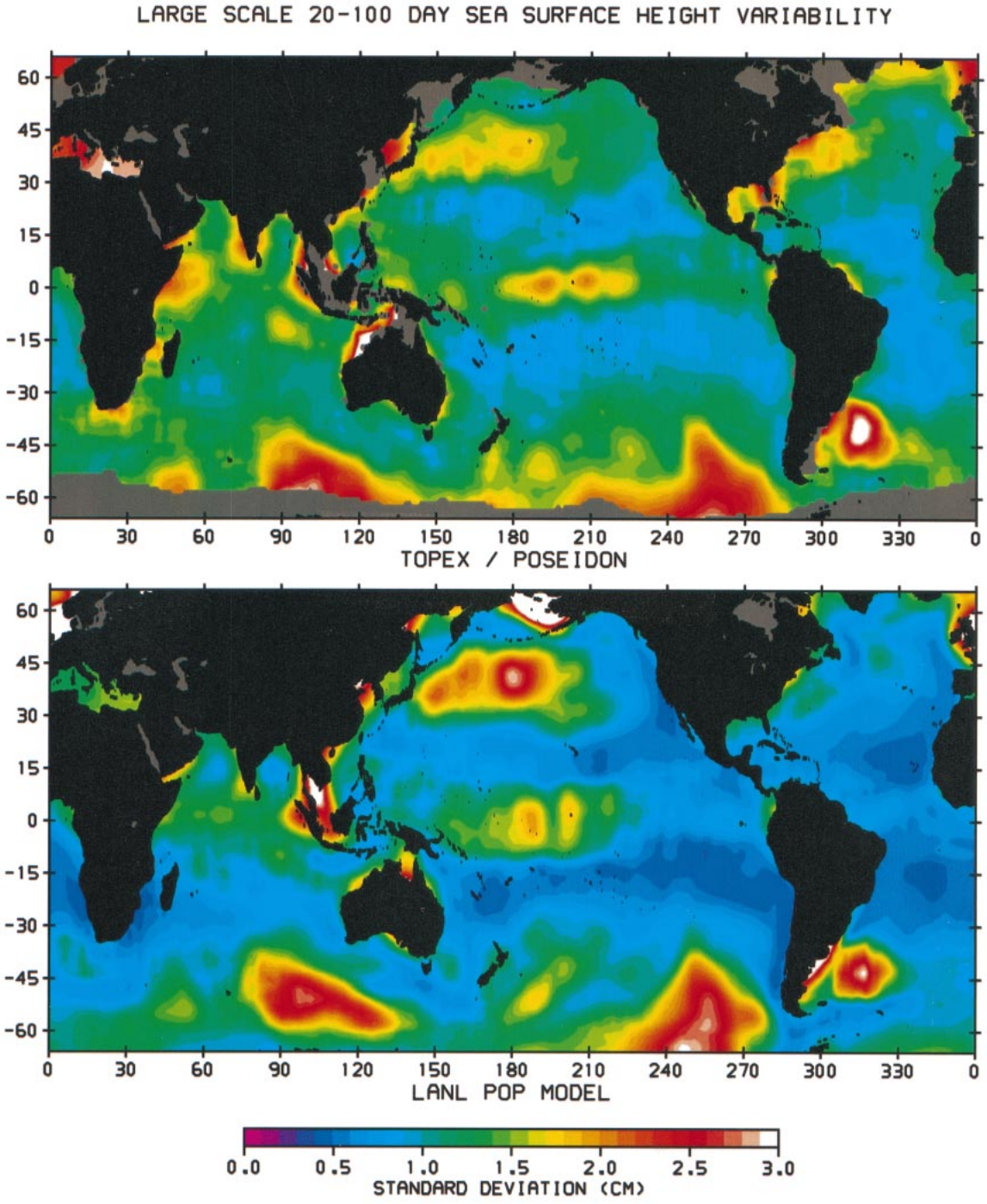

FIG. 1. Root-mean-square variability of sea surface height measured by T/P (top) and simulated by the POP ocean general circulation model (bottom). Both were filtered to retain energy at spatial scales larger than 1000 km and temporal scales from 20 to 100 days. [From Fu and Smith (1996).]

of the orbit errors by fitting the large-scales to an orbit error model (Fu and Vazquez 1988; Wagner and Tai 1994). Such procedures often create distortion of the signals at large scales and compromise the data quality for studying the intraseasonal variability. With its orbit accuracy better than 3 cm (Tapley et al. 1996), T/P provides the first opportunity for observing the large-scale patterns of the variability.

Shown in Fig. 1 is the standard deviation of sea level variability at spatial scales larger than 1000 km and

temporal scales between 20 and 100 days determined from the T/P altimeter observations as well as from the simulation by an ocean general circulation model (from Fu and Smith 1996). The ocean model, developed by the Parallel Ocean Program (POP) of the Los Alamos National Laboratory, has an average spatial resolution of $\frac{1}{5}^\circ$ and 20 vertical levels. The simulation was performed by the model driven by the European Center for Medium-Range Weather Forecasts twice-daily wind stress (smoothed over 3 days) and heat flux climatology. The observed energy level is generally low with an rms amplitude of 2–3 cm. The maximum amplitude is in the Southern Ocean with rms magnitude greater than 3 cm and peak-to-trough sea level variations exceeding 10 cm in certain regions. The geographic distribution of the observed energy level is well reproduced by the model (also see Chao and Fu 1995). In the Northern Hemisphere where the wind forcing is relatively well known, the model is able to simulate the temporal evolution of the variability with a high degree of correlation with observed sea level time series. Chao and Fu (1995) showed that the model-simulated sea level was highly correlated with the model's barotropic streamfunction, suggesting that the variability was caused by barotropic motions. Fukumori et al. (1998) also discussed the geographic distribution of barotropic variability and its temporal scales based on an ocean general circulation model. Fu and Davidson (1995) made an attempt to describe the observed variability in terms of a wind-driven linearized barotropic vorticity equation with only limited success. By filtering out baroclinic waves from altimeter observations, however, Vivier et al. (1999) showed that a significant portion of the intraseasonal variability was consistent with a time-dependent Sverdrup relation.

The details of the intraseasonal variability revealed in the T/P data have not been fully investigated. In this paper we present the results from the investigation of a particular mode of variability in the Argentine Basin of the South Atlantic Ocean where the observed intraseasonal variability has the highest energy level according to Fig. 1. The variability of the circulation of the Argentine Basin has been documented by many previous studies. The region exhibits a high degree of variability over a wide range of spatial and temporal scales. The eddy energy level in the Brazil–Malvinas Confluence region is among the highest in the world's oceans (Provost and Le Traon 1993), with an rms sea level variability greater than 30 cm. Large-scale annual and semiannual cycles are also prominent with a sea level amplitude of 13 and 7 cm, respectively (Fu 1996; Provost and Le Traon 1993). There have been numerous observational and theoretical studies of the eddy and seasonal variabilities of the region (Olson et al. 1988; Garzoli and Garaffo 1989; Matano et al. 1993; Garzoli and Giulivi 1994). Recently, the large-scale interannual variability of the South Atlantic was investigated by Witter and Gordon (1999) using the T/P data. They discovered a distinct interannual mode in the Brazil–Malvinas Confluence region.

There has been relatively little discussion of the intraseasonal variability of the Argentine Basin in the literature. Weatherly (1993) reported the findings of high-frequency (periods of 22–28 days) oscillations in the observations made by current meters near the ocean bottom close to the Zapiola Rise, a sediment ridge located along 45°S from 315°–320°. He suspected that these oscillations were due to large-scale barotropic Rossby waves. In this paper we present a view of the spatial and temporal characteristics of such waves from 5 years of the T/P data.

2. Data processing

TOPEX/Poseidon measures sea surface height (SSH) every 6.2 km along repeat ground tracks every 10 days. The longitudinal distance between adjacent ground tracks is approximately 200 km at the latitude of the Argentine Basin. The time difference between adjacent tracks is about 3 days. Although the Nyquist period for the repeat measurements along a given track is 20 days, the measurements made by adjacent tracks are useful in providing high-frequency (higher than the Nyquist frequency) sampling of the variabilities that have spatial scales larger than the track spacing, such as the tides in the open ocean as well as the intraseasonal variability. For example, data collected within specified bins ($3^\circ \times 3^\circ$) were used to estimate the amplitude and phase of ocean tides at diurnal and semidiurnal periods (e.g., Schrama and Ray 1994). In this study we are pushing the limit of the T/P data in describing the details of the intraseasonal variability.

The T/P Merged Geophysical Data Records (GDR) were processed with the standard corrections applied, including the tidal and inverted-barometer corrections (Callahan 1994). The mean-sea-surface model supplied in the GDR was first removed from individual SSH and the residuals were interpolated to a set of normal points (6.2 km apart) for each repeat track. All the data from October 1992 through December 1997 within a box bounded by 30°–50°S, 300°–335°E were used in the analysis. A record temporal mean was removed from the residual SSH at each normal point. The resultant SSH ''anomalies'' that reflect only the temporal variations formed the database for the study.

To focus on the large scales we need to filter out the mesoscale variability. A Gaussian-weighted smoothing scheme was applied to the data to create smoothed SSH anomaly maps on a uniform $1^\circ \times 1^\circ$ grid every 3 days. At each grid node, all the data within a search window in space and time were used to create a smoothed estimate. The half-weight scale where the Gaussian weight falls to half of the maximum value was set to 1° in latitude, 2° in longitude, and 5 days in time. The search window has a dimension of 3° in latitude, 12° in longitude, and 20 days in time. Such a procedure is an

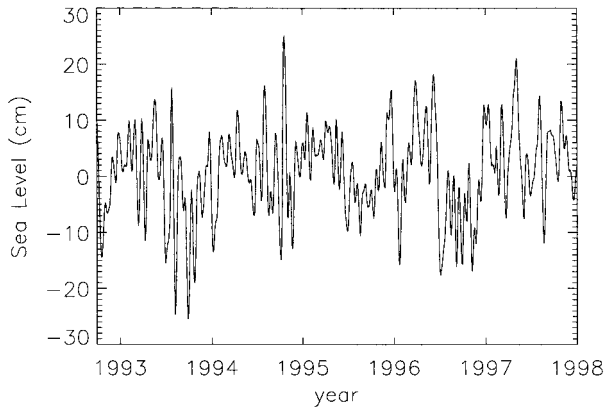

FIG. 2. Time series of the sea surface height anomaly obtained from T/P at 42°S, 316°E.

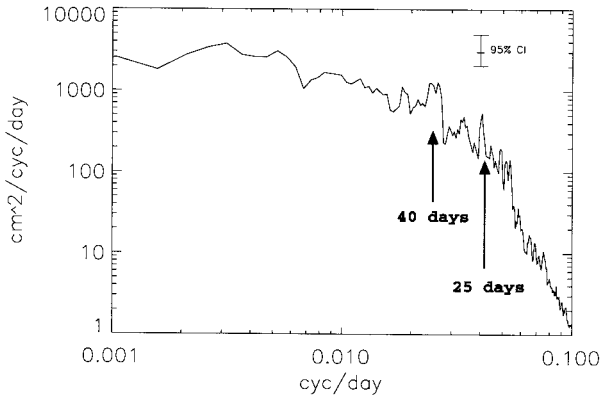

FIG. 3. Spatially averaged frequency spectra of sea level anomaly computed at 1° × 1° grids. The average is performed over a 4° lat × 10° long box centered on 42°S, 316°E. The 95% confidence interval is based on 40 degrees of freedom.

efficient scheme for producing gridded maps of large-scale variabilities. As an illustration of the performance of the scheme, the result of using the scheme to sample a relatively fast-moving, large-scale sinusoidal wave is presented in appendix A. It is shown that large-scale variabilities at frequencies close to the Nyquist of T/P can be sampled qualitatively with a reduced amplitude.

3. Detection of a 25-day oscillation

Displayed in Fig. 2 is the time series of SSH at 42°S, 316°E, near the center of the study domain. An annual cycle superimposed with energetic high-frequency fluctuations is prominent. A spatially averaged (over a 4° latitude × 10° longitude box centered on 42°S, 316°E) frequency spectrum is shown in Fig. 3. It is the average of 40 spectra within the box. Because the scales for the Gaussian smoothing are 1° in latitude and 2° in longitude, only 20 independent estimates are averaged. The degrees of freedom of the averaged spectrum are thus 40 because each independent spectral estimate has 2 degrees of freedom. The corresponding 95% confidence interval is shown in Fig. 3. A distinct peak occurs at a period of 25 days. This peak can be distinguished from the background with a 95% level of confidence. There is also a broader peak at a period of about 40 days. A sharp drop of energy at periods shorter than 20 days reflects the Nyquist period of T/P. The focus of the present study is the phenomenon with periods of 20–30 days that might be related to the high-frequency variability reported in Weatherly (1993).

A Fourier transform was applied to all the SSH anomaly time series in the study domain. To focus on periods shorter than 30 days, each time series was reconstructed by using only the Fourier coefficients with periods shorter than 30 days. Shown in Fig. 4 is the high-passed version of Fig. 2. Fluctuations with peak-to-trough amplitude of 20 cm are seen with seasonal and interannual modulations of the amplitude. The spatial patterns of the high-passed SSH are displayed in Fig. 5 for a duration of 21 days (30 March–20 April 1993). The evolving patterns can be characterized by a spatially coherent, counterclockwise rotating dipole wave. The rotation is apparently centered on the Zapiola Rise indicated by "×" in the images. The peak-to-trough sea level amplitude is about 10 cm over a scale of 1000 km. The rms variability computed using the entire 5 years of data has a maximum value of 3 cm located around 42°S, 313°E (Fig. 6). The contours of the energy level are somewhat aligned with the contours of f/H, suggesting the barotropic nature of the variability.

The technique of complex-valued empirical orthogonal function (CEOF; e.g., Horel 1984) was applied to the entire array of high-passed SSH time series in the study domain to investigate the dominant spatial and temporal characteristics of the variability. The amplitude and phase of the leading CEOF are shown in Fig. 7. This mode accounts for 38% of the total variance. The spatial pattern of the amplitude is similar to the rms variability map (Fig. 6). The spatial pattern of the

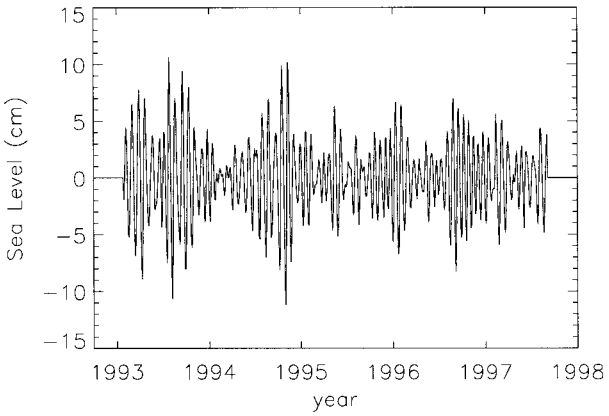

FIG. 4. A high-pass filtered version of Fig. 2. The filtered time series was constructed by using Fourier coefficients with periods shorter than 30 days.

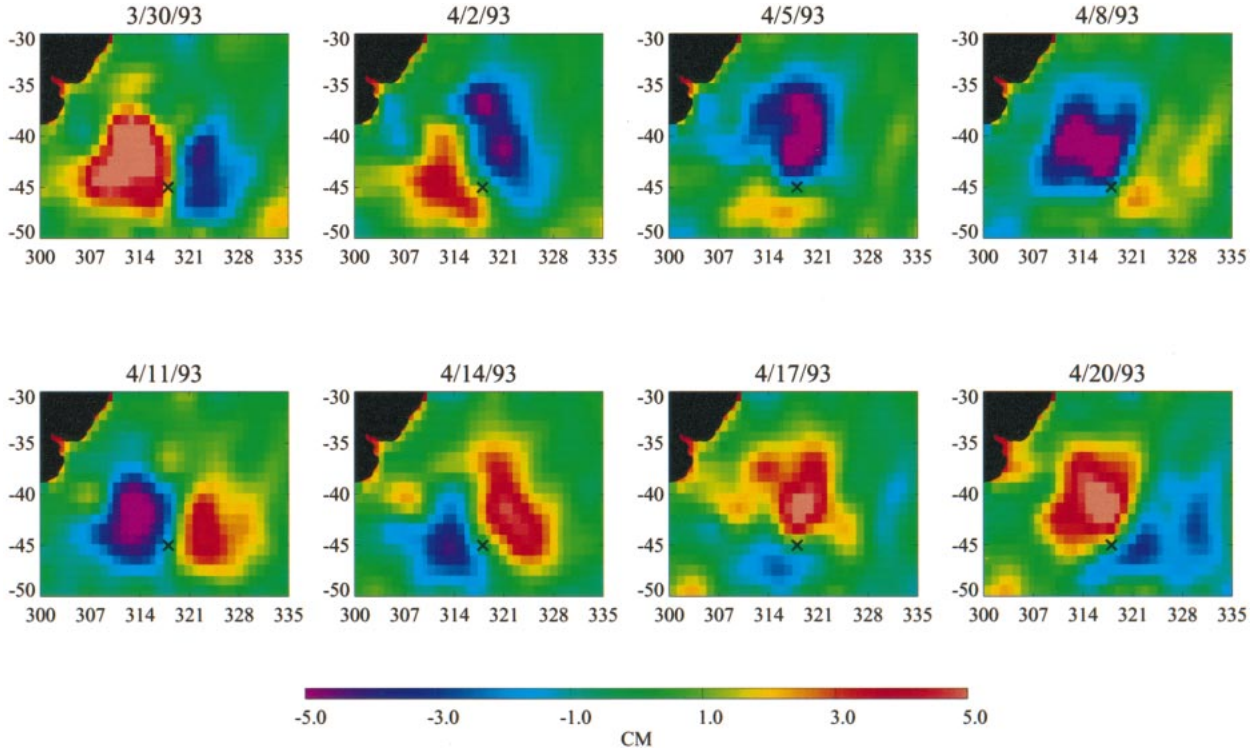

FIG. 5. Snapshots of the high-pass filtered sea surface height anomaly 3 days apart from 30 Mar to 20 Apr 1993. The central location of the Zapiola Rise is indicated by "x" in the images.

phase indicates the rotational character of the variability, with the center of rotation located at 45°S, 318°E, over the Zapiola Rise. The definition of the phase in the CEOF computation indicates that the rotation is counterclockwise as shown in Fig. 5. The temporal evolution of the phase reveals a highly periodic fluctuation with a well-defined frequency of 1 cycle per 25 days. The temporal evolution of the amplitude shows a variety of scales. The low-frequency components are visually consistent with the low-frequency modulation of the time series shown in Fig. 4. The CEOF analysis indicates that the counterclockwise rotating dipole wave shown in Fig. 5 is a persistent feature of the region with a highly variable amplitude.

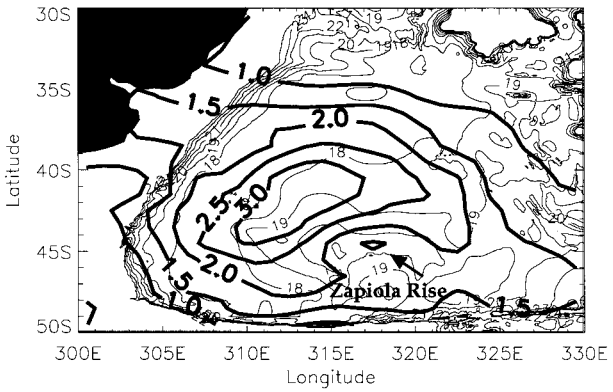

FIG. 6. Root-mean-square amplitude of the high-pass filtered sea surface height variability (thick contours in unit of cm). The f/H contours in units of -1×10^{-9} s^{-1} m^{-1} are shown by the thin lines.

The spatial and temporal scales of the dipole waves indicate that the motion field of the waves is probably barotropic. First, the 1000-km spatial scales of the dipole waves are much larger than the internal Rossby radius of deformation (~30 km). Second, the period of baroclinic Rossby waves with a wavelength of 1000 km is on the order of 4 yr, much longer than the observed period of 25 days. The 25-day waves observed in the T/P data are probably of the same origin as those observed by the deep current meters reported by Weatherly (1993). The current velocity spectra at 10 m above the ocean bottom at 42.5°S, 315°E show peaks at periods close to 25 days in both the zonal and meridional components (Harkema and Weatherly 1989). The coherence between the meridional and zonal components is statistically significant in the 25-day band and the phase indicates a counterclockwise rotating current. Shown in Fig. 8 are the rotary spectra (Gonella 1972) computed from the velocity records of Harkema and Weatherly (1989). The dominance of the counterclockwise component at periods close to 25 days is clearly shown at both 10 and 198 m above the ocean bottom. The counterclockwise component of velocities at the two depths are highly coherent at periods from 20 to 50 days (0.95, above the 95% confidence level with five degrees of

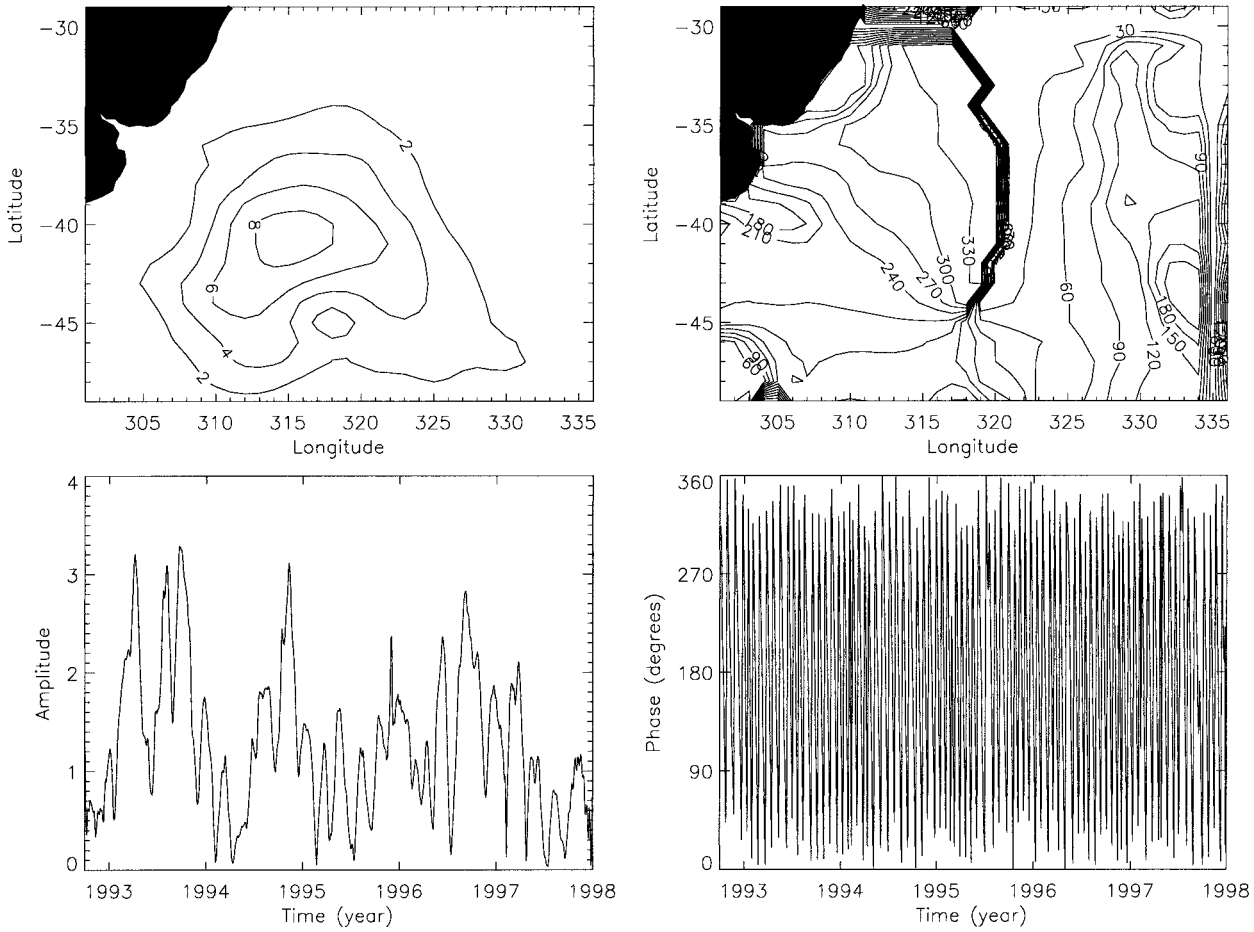

FIG. 7. The first complex-valued empirical orthogonal function for the high-pass filtered sea surface height anomalies. Top left: the spatial distribution of the maximum amplitude in cm attained during the observation period. Bottom left: the temporal evolution of the amplitude in arbitrary unit. Top right: the spatial distribution of the phase in degrees. Bottom right: temporal evolution of the phase in degrees.

freedom) with small phase difference (Fig. 9). The spectral analysis suggests that a vertically coherent, counterclockwise rotating current with a period of about 25 days does exist near the ocean bottom in the vicinity of the Zapiola Rise. According to the sea-level patterns shown in Figs. 5 and 7, the geostrophic currents associated with the 25-day waves detected by T/P also rotate in a counterclockwise sense in the region of the current meters. The current meter observations are thus consistent with the T/P observations.

The magnitude of the current variability is on the order of 1 cm s^{-1}, computed from the sea surface slope of a 10-cm change over a distance of 1000 km based on geostrophy. However, the amplitude of the current variability estimated from the current-meter spectra (Fig. 8) is about 2 cm s^{-1} in the period band of 20–30 days. The difference between the two estimates is consistent with the fact that T/P has undersampled the 25-day variability and resulted in underestimation of the variability (see appendix A). The variability of the total mass transport caused by the weakly varying current is enormous because the movement involves the entire water column. Even a 1 cm s^{-1} fluctuation can create a change in mass transport on the order of 50 Sv (Sv $\equiv 10^6$ m^3 s^{-1}), a significant fraction of the transport of the mean flow in the region (Saunders and King 1995).

4. Theoretical considerations

The f/H contours (Fig. 6) are indicators of the gradient of barotropic potential vorticity in the region. Some of the contours are closed around the Zapiola Rise. The fact that the dipole waves are essentially rotating around the Zapiola Rise (Figs. 5 and 7) suggests their origin as topographically controlled Rossby waves dictated by the f/H contours. As discussed in the preceding section, the observed waves are evidently barotropic and can be described by the linearized barotropic potential vorticity equation:

$$\frac{\partial}{\partial t}\left(\nabla^2\eta - \frac{f^2}{gH}\eta\right) + HJ\left(\eta, \frac{f}{H}\right) = 0, \qquad (1)$$

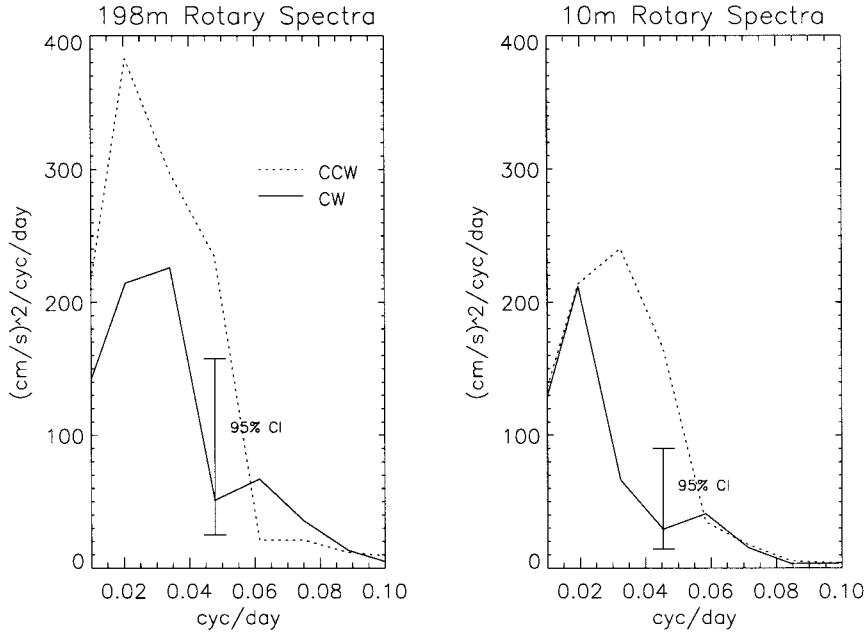

FIG. 8. The rotary components of the frequency spectra of velocity records from moored current meters at 10 m (right) and 198 m (left) from the bottom of the ocean. The clockwise (CW) components are shown by the solid lines and the counterclockwise (CCW) components by the dotted lines. The 95% confidence intervals based on 10 degrees of freedom are shown for the spectral estimate at a period of 22 days.

where η is the sea surface height anomaly, H is the ocean depth (a variable), f is the Coriolis parameter, and J is the Jacobian operator. For the scales of the observed waves, which are on the order of 1000 km, the term $f^2\,\eta/gH$ can be neglected when compared to $\nabla^2\eta$. The geometry of the solution is dictated by the second term of (1), the advection of the potential vorticity. Given the patterns of the contours of f/H and the apparent rotation of the waves around the Zapiola Rise, we approximate f/H by an axial symmetric function in

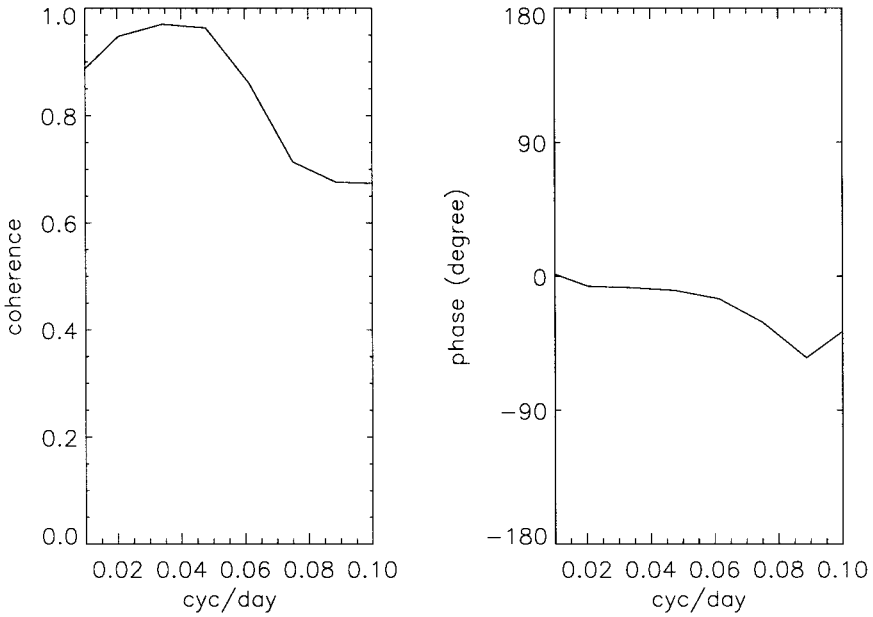

FIG. 9. The amplitude (left) and phase (right) of the coherence between the counterclockwise components of current velocity records at 10 and 198 m above the ocean bottom.

order to obtain an analytic solution to (1). Equation (1) can then be converted into polar coordinates centered on the Zapiola Rise:

$$\frac{\partial}{\partial t}\left(\frac{\partial^2\eta}{\partial r^2} + \frac{1}{r}\frac{\partial\eta}{\partial r} + \frac{1}{r^2}\frac{\partial^2\eta}{\partial\theta^2}\right) - \frac{H}{r}\frac{\partial\eta}{\partial\theta}\frac{\partial}{\partial r}\left(\frac{f}{H}\right) = 0. \quad (2)$$

We seek an azimuthally propagating wave solution,

$$\eta = p(r)\exp[i(s\theta - \omega t)],$$

where s is the azimuthal wavenumber and ω is the wave frequency. We define

$$\beta_e \equiv H\frac{\partial}{\partial r}\left(\frac{f}{H}\right),$$

which represents an equivalent beta effect. In order to obtain an analytic solution, we assume that β_e is a constant. Although β_e does vary by about 30% in the region, this approximation is probably within the same extent of the approximation of axial symmetry discussed earlier. Equation (2) then becomes

$$\frac{\partial^2 p}{\partial r^2} + \frac{1}{r}\frac{\partial p}{\partial r} - \frac{s^2}{r^2}p + \frac{s}{r}\frac{\beta_e}{\omega}p = 0. \quad (3)$$

With $z \equiv 2\sqrt{r}$, (3) can be transformed to

$$\frac{\partial^2 p}{\partial z^2} + \frac{1}{z}\frac{\partial p}{\partial z} - \frac{4s^2}{z^2}p + \frac{s\beta_e}{\omega}p = 0, \quad (4)$$

which is a Bessel equation. A general solution to (4) can be written as

$$\eta = \sum_{s=0}^{\infty} A_s \exp[i(s\theta - \omega t)]J_{2s}(2k\sqrt{r}), \quad (5)$$

where $k^2 = s\beta_e/\omega$. Note that β_e is positive in this case; namely, f/H is increasing with r due to the increasing depth outward from the center (note that f is negative in the Southern Hemisphere). This leads to a counterclockwise rotating wave solution as observed (s and ω are of the same sign). If β_e is negative, the wave solution would show clockwise rotation. Because the observed waves assume a dipole structure, we set $s = 1$. That the observed waves are confined to the Argentine Basin where there are closed f/H contours leads us to require the solution to be confined to a circular region with a radius of L. To the extent of the approximation underlying this solution, we simply set the first zero crossing of η at L:

$$J_2(2k\sqrt{L}) = 0 \quad \text{or} \quad 2k\sqrt{L} = 5.15. \quad (6)$$

From (6) the wave period is given by

$$T = \frac{2\pi}{\omega} = \frac{5.15^2\pi}{2L\beta_e}. \quad (7)$$

The value of β_e estimated from Fig. 6 is $(3.3 \pm 1) \times 10^{-11}$ s^{-1} m^{-1} in the vicinity of the Zapiola Rise. Physically, L is determined by the scale over which the f/H contours either change abruptly (i.e., a potential vorticity barrier) or flatten out (i.e., no potential vorticity gradient to support Rossby waves). Estimated from Fig. 6, L is on the order of 500 km. With these values for L and β_e, $T \approx 30$ days. Figure 10 shows that T is not particularly sensitive to either L or β_e; it varies from 20 to 40 days within about 30% change of the two parameters. The observed wave period of 25 days can be readily explained by the theory. Shown in Fig. 11 is the wave function with the above parameters for $s = 1$. The spatial patterns of the observed waves can also be qualitatively accounted for by the theory.

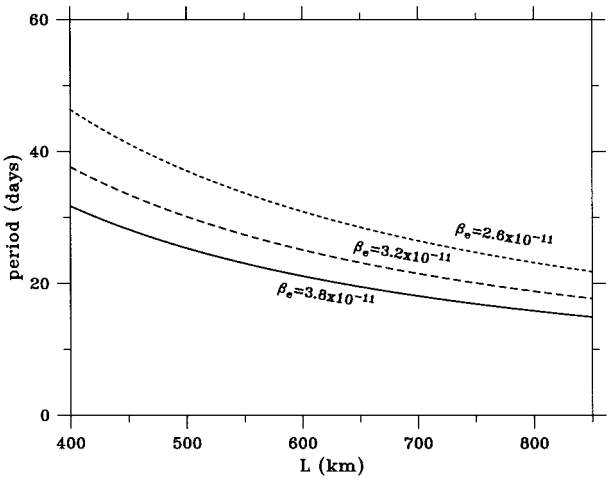

FIG. 10. The wave period determined from (7) as a function of L for three values of β_e.

The theoretical analysis discussed above suggests that the observed waves are signatures of a normal mode associated with the local topography. To verify the existence of such a mode in a more realistic setting, a numerical model was run to simulate the variabilities of the Argentine Basin. This is a barotropic, primitive-equation model with a spatial resolution of 0.5° × 0.5°, covering the domain of 20°–60°S, 285°–345°E. The resolution of this model is about 1/20 of the scale of the observed waves and is thus deemed adequate for the problem. All the model boundaries are closed. The eddy viscosity coefficient used in the model is 500 m^2 s^{-1} in the interior domain. It increases to 5000 m^2 s^{-1} near the model's open boundaries in order to minimize spurious boundary Kelvin waves. The model topography is based on the ETOPO5 database. The daily wind fields produced by the National Centers for Environmental Prediction (NCEP) were used to drive the model from 1 January 1990 to 31 December 1997. The 8-yr mean wind was removed because the mean circulation is not of interest to the study. CEOF analysis was applied to the resulting barotropic streamfunction. The first three leading modes account for 62% of the variance. The first two, with periods of 10–20 days, are not confined to the region of the Zapiola Rise. They are not visible in the T/P data probably because their frequencies are

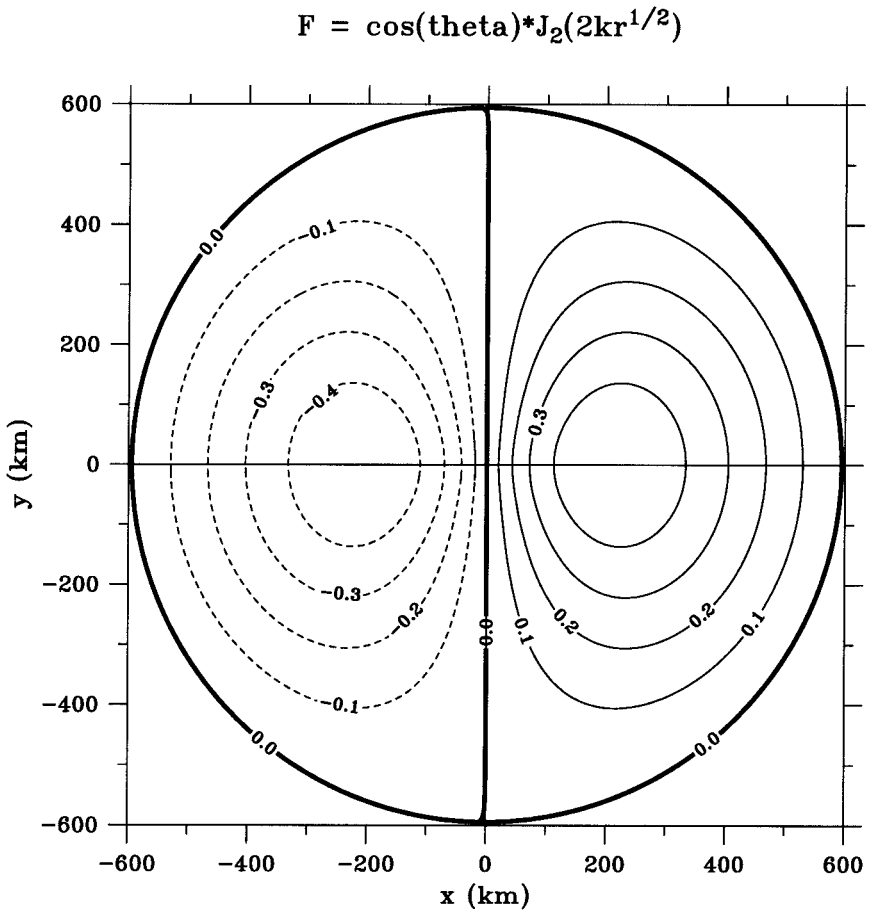

FIG. 11. The spatial pattern of the wave function represented by (5) with $s = 1$.

generally higher than T/P's Nyquist frequency. The third mode, accounting for 10% of the variance, has a distinct period of 22 days with spatial patterns similar to the observed 25-day waves (Fig. 12). In order to examine the relationship of this mode to the bottom topography, we ran a similar experiment in which the bottom was flat. The 22-day mode then disappeared while the other two were still present. The degree of resemblance in both the spatial phase and amplitude distribution between Figs. 7 and 12 is fairly convincing. The maximum sea level amplitude associated with the mode is about 8 cm, comparable to the observation. The first two modes, if real, would have aliasing effects on the sampling of the third mode by T/P because their frequencies are higher than T/P's Nyquist frequency. However, the visual resemblance between the observations and the simulated third mode suggests that the possible aliasing effects are not significant.

5. Summary and discussion

Satellite altimetry provides the first synoptic view of the large-scale intraseasonal variability of the ocean. Due to the sparseness of in situ observations, our knowledge of the spatial extent and pattern of the variability has been sketchy. The T/P altimeter is the first that has sufficient accuracy for observing the variability, although its sampling capability is only marginal. This paper presents a case study of the Argentine Basin where intraseasonal variability is particularly energetic. Near the highest frequencies resolvable by T/P, a 25-day rotating dipole wave is detected. The scale of the wave is about 1000 km with a peak-to-trough amplitude of 10 cm. Due to the closeness of the period to the Nyquist period of T/P (20 days), the amplitude may have been underestimated by 30%–40%. The wave rotates counterclockwise around the Zapiola Rise. The spatial and temporal characteristics of the wave can be explained by the solution of a linearized barotropic vorticity equation. The observed wave appears to be a normal mode associated with the local f/H geometry. Deep current-meter observations provide corroborative evidence for the altimetric observations and the interpretation of them as barotropic waves.

Observational as well as theoretical and numerical studies of the Argentine Basin have indicated the existence of an anticyclonic (counterclockwise) mean circulation around the Zapiola Rise (Flood and Shor 1988;

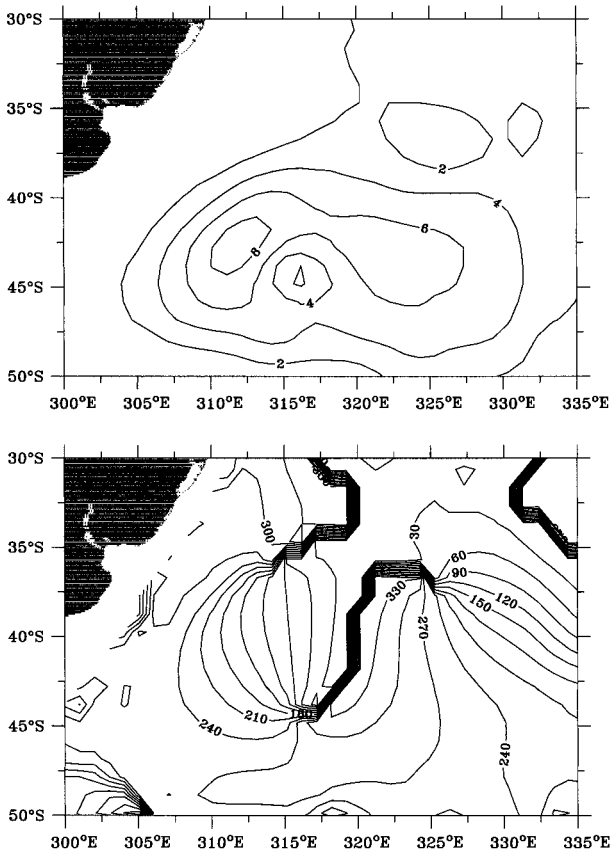

FIG. 12. The spatial patterns of the amplitude (top) and the phase (bottom, in degrees) for the third CEOF of the model simulation. The amplitudes shown are the maximum values in cm attained during the simulation.

Saunders and King 1995; Weatherly 1993; Dewar 1998; de Miranda et al. 1999). The transport of this anticyclone is estimated to be 140 Sv. Theoretical and modeling analysis suggests that this mean flow is driven by eddies trapped inside closed f/H contours around the Zapiola Rise. The counterclockwise dipole wave observed in the present study might have some interactive relationship with the anticyclonic mean flow.

In an effort to investigate the relationship between the variability of the wind field and the observed sea level variability, we have examined the time series of wind stress and its curl in the Argentine Basin. Data from both the NCEP analysis and the European Remote Sensing Satellite scatterometer were used for the analysis. There was no evidence for any significant wind variability at periods close to 25 days. Wavelet analysis was also performed to the variance of wind stress curl at periods close to 25 days. We found no significant correlation between the variability of the wave amplitude with the variability of the wind stress curl. Therefore we are not able to establish any relationship between wind forcing and the observed wave. This of course may have something to do with the quality of the wind observations. On the other hand, because the wave appears to be a normal mode of the basin, it is probably excited as a resonant response to random forcing from a variety of sources.

Recent modeling studies (Fukumori et al. 1998; Stammer et al. 2000; Tierney et al. 2000) have suggested that there is a significant amount of variability of sea level and ocean currents at periods shorter than the Nyquist period of T/P. This is also demonstrated by the high-frequency modes of the model simulation discussed in the preceding section. These high-frequency variabilities could be aliased into lower frequencies and cause some errors in the present analysis. Such errors may have contributed to the uncertainty in the estimation of the wave amplitudes, but they do not appear to have major effects on the interpretation of the observed 25-day oscillations, which have been confirmed by both the current-meter observations and the theoretical and modeling analysis.

Acknowledgments. The current meter data were kindly provided by Dr. Georges Weatherly of the Florida State University. Comments from the review of an earlier version by Drs. Carl Wunsch, Phil Woodworth, as well as from two anonymous reviewers have greatly improved the quality of the presentation. The research presented in the paper was partly carried out by the Jet Propulsion Laboratory, California Institute of Technology, under contract with the National Aeronautic and Space Administration. Support from the TOPEX/Poseidon project is acknowledged. The effort of Bo Qiu was supported by TOPEX/Poseidon Extended Mission through Contract 960889 issued to the University of Hawaii.

APPENDIX

Sampling of High-Frequency Large-Scale Variability by TOPEX/Poseidon

To investigate how well T/P is able to sample a fast-moving, large-scale anomaly, we conducted an experiment in which a simulated plane wave was sampled at real T/P measurement times and locations. The simulated observations were then used to reconstruct the wave for comparison to the truth. The simulated sea surface height anomaly is given by

$$h = A \sin\left(\frac{2\pi}{L_x}x + \frac{2\pi}{L_y}y - \frac{2\pi}{P}t\right),$$

where $A = 5$ cm, $L_x = 25°$, $L_y = 15°$, and $P = 25$ days. This wave was sampled over 40 days in the Argentine Basin at real T/P measurement times and locations. The simulated data were processed using the Gaussian smoothing scheme described in section 2 to produce $1° \times 1° \times 3$ day maps. Shown in Fig. A1 is a comparison of the simulated T/P-sampled wave with the truth for four consecutive 3-day maps. The correlation between

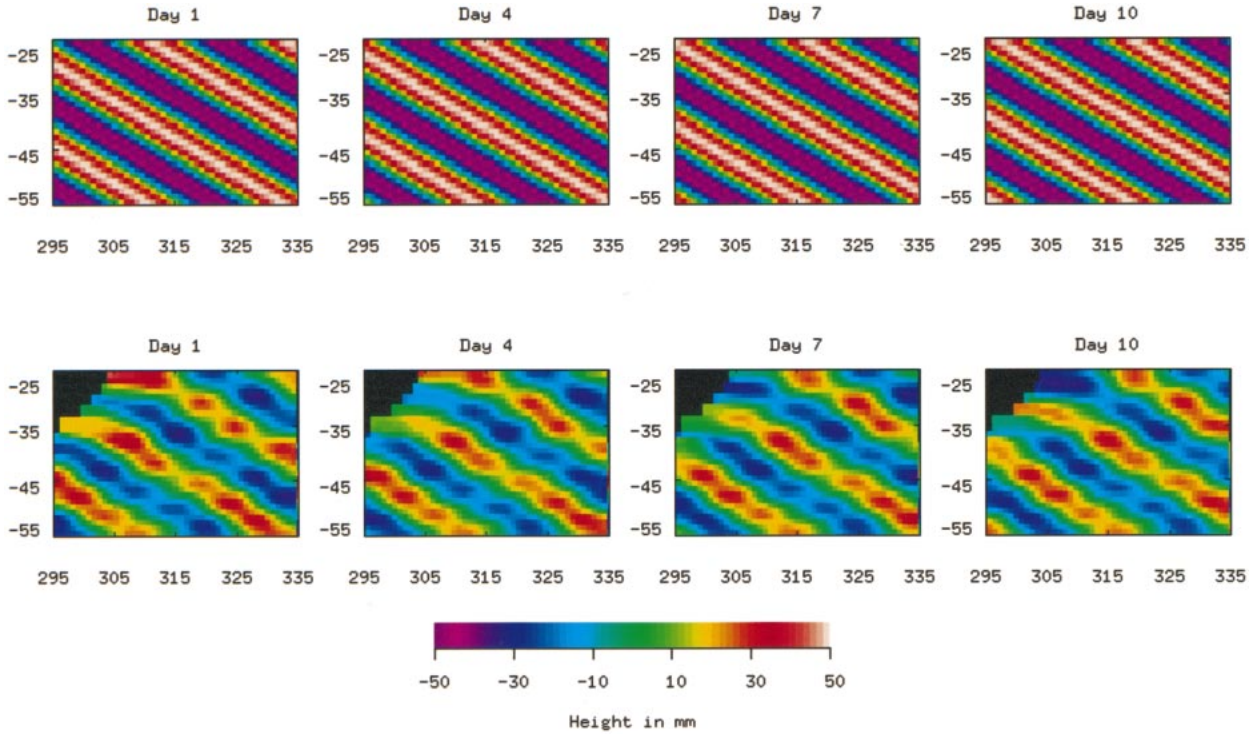

FIG. A1. Simulated sinusoidal waves (upper panels) vs their reconstructions based on values sampled by T/P along its ground tracks at overflight times (lower panels). Each box represents the domain of study with the vertical axis in degrees of latitude and horizontal axis in degrees of longitude.

each pair is greater than 0.85. The rms difference is about 2 cm. The wave amplitude is undersampled by the simulated T/P observations by about 30%–40%, but the basic pattern and its propagation characteristics are faithfully reproduced. This experiment has demonstrated that large-scale, high-frequency sea-level variations can be mapped qualitatively by T/P at time intervals shorter than the 10-day repeat period. However, the experiment indicates that the amplitude of the variations might be underestimated. Therefore, the amplitude of the 25-day waves might be larger than estimated from T/P data.

REFERENCES

Brink, K. H., 1989: Evidence for wind-driven current fluctuations in the western North Atlantic. *J. Geophys. Res.,* **94,** 2029–2044.

Callahan, P. S., 1994: TOPEX/Poseidon GDR user's handbook. Jet Propulsion Laboratory Document JPL-D-8944, 84 pp.

Chao, Y., and L.-L. Fu, 1995: A comparison between the TOPEX/Poseidon data and a global ocean general circulation model during 1992–93. *J. Geophys. Res.,* **100,** 24 965–24 976.

de Miranda, A. P., B. Barnier, and W. K. Dewar, 1999: On the dynamics of the Zapiola Anticyclone. *J. Geophys. Res.,* **104,** 21 137–21 150.

Dewar, W. K., 1998: Topography and barotropic transport control by bottom friction. *J. Mar. Res.,* **56,** 295–328.

Enfield, D. B., 1987: The intraseasonal oscillation in eastern Pacific sea levels: How is it forced? *J. Phys. Ocenaogr.,* **17,** 1860–1867.

Flood, R. D., and A. N. Shor, 1988: Mud waves in the Argentine Basin and their relationship to regional bottom circulation patterns. *Deep-Sea Res.,* **35,** 943–971.

Fu, L.-L., 1996: The circulation and its variability of the South Atlantic Ocean: First results from the TOPEX/Poseidon mission. *The South Atlantic: Present and Past Circulation,* G. Wefer et al., Eds., Springer-Verlag, 63–82.

——, and J. Vazquez, 1988: On correcting radial orbit errors for altimetric satellites using crossover analysis. *J. Atmos. Oceanic Technol.,* **5,** 466–471.

——, and R. A. Davidson, 1995: A note on the barotropic response of sea level to time-dependent wind forcing. *J. Geophys. Res.,* **100,** 24 955–24 963.

——, and R. D. Smith, 1996: Global ocean circulation from satellite altimetry and high-resolution computer simulation. *Bull. Amer. Meteor. Soc.,* **77,** 2625–2636.

——, E. J. Christensen, C. A. Yamarone, M. Lefebvre, Y. Ménard, M. Dorrer, and P. Escudier, 1994: TOPEX/Poseidon Mission Overview. *J. Geophys. Res.,* **99,** 24 369–24 381.

Fukumori, I., R. Raghunath, and L.-L. Fu, 1998: The nature of global large-scale sea level variability in relation to atmospheric forcing: A modeling study. *J. Geophys. Res.,* **103,** 5493–5512.

Garzoli, S. L., and Z. Garraffo, 1989: Transports, frontal motions and eddies at the Brazil–Malvinas confluence as revealed by inverted echo sounders. *Deep-Sea Res.,* **36,** 681–703.

——, and C. Giulivi, 1994: What forces the variability of the south western Atlantic boundary currents? *Deep-Sea Res.,* **41,** 1527–1550.

Gonella, J., 1972: A rotary-component method for analyzing meteorological and oceanographic vector time series. *Deep-Sea Res.,* **18,** 775–788.

Harkema, R., and G. L. Weatherly, 1989: A compilation of moored current meter data in the Argentine Basin April 25, 1987–March 14, 1988. Tech. Rep. CMF-89-01, Dept. of Oceanography, The Florida State University, Tallahassee, FL, 64 pp.

Horel, J. P., 1984: Complex principal component analysis: Theory and examples. *J. Climate Appl. Meteor.,* **23,** 1600–1673.

Koblinsky, C. J., P. P. Niiler, and W. J. Schmitz Jr., 1989: Observations of wind-forced deep ocean currents in the North Pacific. *J. Geophys. Res.,* **94,** 10 773–10 790.

Luther, D. S., A. D. Chave, J. H. Filloux, and P. F. Spain, 1990: Evidence for local and nonlocal barotropic responses to atmospheric forcing during bempex. *Geophys. Res. Lett.,* **17,** 949–952.

Matano, R. P., M. G. Schlax, and D. B. Chelton, 1993: Seasonal variability in the southwestern Atlantic. *J. Geophys. Res.,* **98,** 18 027–18 035.

McPhaden, M. J., 1996: Monthly period oscillations in the Pacific North Equatorial Countercurrent. *J. Geophys. Res.,* **101,** 6337–6359.

Niiler, P. P., J. Filloux, W. T. Liu, R. M. Samelson, J. D. Paduan, and C. A. Paulson, 1993: Wind-forced variability of the deep eastern North Pacific: Observations of seafloor pressure and abyssal currents. *J. Geophys. Res.,* **98,** 22 589–22 602.

Olson, D. B., G. P. Podesta, R. H. Evans, and O. B. Brown, 1988: Temporal variations in the separation of Brazil and Malvinas Currents. *Deep-Sea Res.,* **35,** 1971–1990.

Provost, C., and P.-Y. Le Traon, 1993: Spatial and temporal scales in altimetric variability in the Brazil–Malvinas Current Confluence region: Dominance of the semiannual period and large spatial scales. *J. Geophys. Res.,* **98,** 18 037–18 051.

Samelson, R. M., 1990: Evidence for wind-driven current fluctuations in the eastern North Atlantic. *J. Geophys. Res.,* **95,** 11 359–11 368.

Saunders, P. M., and B. A. King, 1995: Bottom currents derived from a shipborne ADCP on the WOCE Cruise A11 in the South Atlantic. *J. Phys. Oceanogr.,* **25,** 329–347.

Schrama, E. J. O., and R. D. Ray, 1994: A preliminary tidal analysis of TOPEX/Poseidon altimetry. *J. Geophys. Res.,* **99,** 24 799–24 808.

Stammer, D., C. Wunsch, and R. M. Ponte, 2000: De-aliasing of global high frequency barotropic motions in altimeter observations. *Geophys. Res. Lett.,* **27,** 1175–1178.

Tapley, B. D., and Coauthors, 1996: The Joint Gravity Model 3. *J. Geophys. Res.,* **101,** 28 029–28 049.

Tierney, C., J. Wahr, F. Bryan, and V. Zlotnicki, 2000: Short-period oceanic circulation: Implications for satellite altimetry. *Geophys. Res. Lett.,* **27,** 1255–1258.

Vivier, F., K. A. Kelly, and L. Thompson, 1999: Contributions of wind forcing, waves, and surface heating to sea-surface height observations in the Pacific Ocean. *J. Geophys. Res.,* **104,** 20 767–20 788.

Wagner, C. A., and C. K. Tai, 1994: Degradation of ocean signals in satellite altimetry due to orbit removal processes. *J. Geophys. Res.,* **99,** 16 255–16 267.

Weatherly, G. L., 1993: On deep-current and hydrographic observations from a mudwave region and elsewhere in the Argentine Basin. *Deep-Sea Res.,* **40** (Part II), 851–858.

Witter, D. L., and A. L. Gordon, 1999: Interannual variability of South Atlantic circulation from 4 years of TOPEX/Poseidon altimeter observations. *J. Geophys. Res.,* **104,** 20 927–20 948.

Wunsch, C., and A. E. Gill, 1976: Observations of equatorially trapped waves in Pacific sea level variations. *Deep-Sea Res.,* **23,** 371–390.